Research Article

Cancer Immunology Research

PVRIG and PVRL2 Are Induced in Cancer and Inhibit CD8$^+$ T-cell Function

Sarah Whelan[1], Eran Ophir[2], Maya F. Kotturi[1], Ofer Levy[2], Sudipto Ganguly[3], Ling Leung[1], Ilan Vaknin[2], Sandeep Kumar[1], Liat Dassa[2], Kyle Hansen[1], David Bernados[1], Benjamin Murter[3], Abha Soni[3], Janis M. Taube[3], Amanda Nickles Fader[4], Tian-Li Wang[4], Ie-Ming Shih[4], Mark White[1], Drew M. Pardoll[3], and Spencer C. Liang[1]

Abstract

Although checkpoint inhibitors that block CTLA-4 and PD-1 have improved cancer immunotherapies, targeting additional checkpoint receptors may be required to broaden patient response to immunotherapy. PVRIG is a coinhibitory receptor of the DNAM/TIGIT/CD96 nectin family that binds to PVRL2. We report that antagonism of PVRIG and TIGIT, but not CD96, increased CD8$^+$ T-cell cytokine production and cytotoxic activity. The inhibitory effect of PVRL2 was mediated by PVRIG and not TIGIT, demonstrating that the PVRIG–PVRL2 pathway is a nonredundant signaling node. A combination of PVRIG blockade with TIGIT or PD-1 blockade further increased T-cell activation. In human tumors, PVRIG expression on T cells was increased relative to normal tissue and trended with TIGIT and PD-1 expression. Tumor cells coexpressing PVR and PVRL2 were observed in multiple tumor types, with highest coexpression in endometrial cancers. Tumor cells expressing either PVR or PVRL2 were also present in numbers that varied with the cancer type, with ovarian cancers having the highest percentage of PVR$^-$PVRL2$^+$ tumor cells and colorectal cancers having the highest percentage of PVR$^+$PVRL2$^-$ cells. To demonstrate a role of PVRIG and TIGIT on tumor-derived T cells, we examined the effect of PVRIG and TIGIT blockade on human tumor-infiltrating lymphocytes. For some donors, blockade of PVRIG increased T-cell function, an effect enhanced by combination with TIGIT or PD-1 blockade. In summary, we demonstrate that PVRIG and PVRL2 are expressed in human cancers and the PVRIG–PVRL2 and TIGIT–PVR pathways are nonredundant inhibitory signaling pathways.

See related article on p. 244

Introduction

Endogenous immune responses shape the initiation, progression, and suppression of cancer (1, 2). In many solid tumors, effector T cells have an exhausted phenotype within the tumor microenvironment (TME; ref. 3) and cannot mediate an effective antitumor response. Such exhausted T cells can be identified by increased surface expression of coinhibitory receptors, such as PD-1 and CTLA-4, as well as a transcription factor profile characterized by high Eomes and low T-bet expression (4, 5). Antibodies that inhibit interactions of these coinhibitory receptors with their cognate ligands have shown clinical efficacy in patients with advanced cancers (6). Targeting these coinhibitory receptors leads to the expansion of preexisting tumor-reactive T cells and to the generation of T-cell pools with widened T-cell receptor diversity (7–9). Although immune-checkpoint inhibitors have revolutionized cancer treatment, most patients do not respond to treatment and many that respond initially ultimately develop acquired resistance (10). Consequently, increased understanding of the immune response in cancer and identification of additional checkpoint pathways may increase therapeutic treatment options.

CTLA-4 and PD-1 represent the initial members of a growing list of lymphocyte inhibitory pathways. Among these additional pathways, members of the nectin and nectin-like family, including DNAM-1 (CD226), CD96 (TACTILE), TIGIT, and PVRIG (CD112R; refs. 11–13), are under investigation as targets for cancer immunotherapies. DNAM-1 is a costimulatory receptor that binds to 2 ligands, PVR (CD155) and PVRL2 (CD112) (14). Counteracting DNAM-1 signaling are TIGIT, CD96, and PVRIG, receptors that inhibit lymphocyte cell signaling (15, 16). Of these receptors, TIGIT is the best characterized. TIGIT has a high affinity to PVR and a weaker affinity to PVRL2 and PVRL3 and inhibits both T-cell and NK cell responses (17, 18). Blockade of TIGIT improved antitumor responses *in vivo* in preclinical mouse models treated with anti–PD-1 (19). PVR is also a ligand for CD96, which activates human NK cells but inhibits mouse NK cell function (20, 21). A role for CD96 in regulating human T-cell responses is not well understood. PVRIG binds with high affinity to PVRL2 and suppresses T-cell function (13, 22). A direct comparison of the effects mediated by receptors in this family on effector CD8$^+$ T cells has not been reported.

[1]Compugen, USA, Inc., South San Francisco, California. [2]Compugen Ltd, Holon, Israel. [3]Bloomberg Kimmel Institute for Cancer Immunotherapy, Johns Hopkins University, Baltimore, Maryland. [4]Department of Gynecology and Obstetrics, Johns Hopkins University School of Medicine, Baltimore, Maryland.

Note: Supplementary data for this article are available at Cancer Immunology Research Online (http://cancerimmunolres.aacrjournals.org/).

Current address for L. Leung: Celgene, San Francisco, California; current address S. Kumar: Merrimack Pharma, Cambridge, Massachusetts; and current address for S.C. Liang: Alector, South San Francisco, California.

Corresponding Author: Spencer C. Liang, Compugen Inc., USA, 250 East Grand Avenue, Suite 65, South San Francisco, CA 94080. Phone: 415-373-1046; E-mail: spencerl@cgen.com

doi: 10.1158/2326-6066.CIR-18-0442

Although human PVRIG inhibits T-cell responses, the role of PVRIG in T-cell–mediated cancer immunity has not been reported. Furthermore, the expression profile of PVRIG and PVRL2 in human tumors and how it differs from the TIGIT and PD-1 pathways is not well understood. We developed reagents to study this pathway and demonstrate that PVRIG and TIGIT are nonredundant inhibitory receptors within this family on $CD8^+$ T cells and identify cancer types where targeting these pathways may enhance antitumor responses.

Materials and Methods

Protein reagents and cell lines

Anti-PVRIG was generated via hybridoma technology by immunizing mice with human PVRIG Fc and screening for antibodies that bind to human PVRIG and disrupt PVRIG–PVRL2 interactions. COM701 is a humanized anti-PVRIG hinge-stabilized IgG4. Antibodies used for functional studies are described in Supplementary Table S5. Mel-624 cells were obtained from the National Institutes of Health in 2015, and Panc.05.04 cells were obtained from ATCC in 2017. Cells were maintained in culture fewer than 10 passages. Ectopic expression of human PVRIG, human TIGIT, luciferase reporter gene, or a cell-surface anti-CD3 construct (23) was performed by lentivirus transduction (Systems Biosciences). These cell lines were not further authenticated. Cell lines were not contaminated by *Mycoplasma* before and after experiments.

Expression studies in tumor and peripheral immune cells

Healthy donor peripheral blood mononuclear cells (PBMCs) were provided by Stanford University in accordance with the Declaration of Helsinki. Human tissues were provided by the Cooperative Human Tissue Network (CHTN), a National Cancer Institute supported resource, or by Johns Hopkins Hospital (Baltimore, MD) as part of a study that was reviewed and approved by the Johns Hopkins Institutional Review Board. For samples from CHTN, other investigators may have received samples from these same tissue specimens. Upon receipt, tissues were dissociated into single cells by gentleMACS (Miltenyi Biotec) and first stained with Aqua Live Dead (Thermo Fisher) and a cocktail of antibodies (Abs) to CD16 (BioLegend), CD32 (Thermo Fisher), and CD64 (BioLegend) to block Fc receptors. Antibodies to lineage markers were used at 1 μg/mL or at the manufacturer's recommendation (Supplementary Table S1). All isotype control antibodies and target-specific antibodies were used at 5 μg/mL final concentration. In some experiments, cells were stained with anti-PVRIG PE, fixed, permeabilized, and then stained with anti-PVRIG Alexa Fluor 647 or with anti-T-bet or anti-Eomes. Samples were acquired on the BD Fortessa flow cytometer. Analysis was done using FlowJo and gating lineages defined in Supplementary Table S2. For each cell subset with $\geq$100 cells, MFI values were exported, and a fold expression value was calculated by dividing the MFI of a target by the MFI of the relevant isotype control. For a given tumor type, not all subsets had enough cells for analysis. The tumor type was determined based on reviewing the pathology report for each sample and summarized in Supplementary Tables S3 and S4. Internalization of PVRIG and TIGIT was assessed by staining cells with anti-PVRIG and anti-TIGIT at 4°C for 30 minutes, followed by washing and incubation at 37°C. At several time points, cells were transferred to 4°C and stained with anti-human IgG4 to detect the amount of anti-PVRIG or anti-TIGIT remaining on the cell surface.

For IHC studies, an anti-PVRL2 (Sigma HPA-012759) was identified to stain tissue microarrays (BioChain Institute) or triple-negative breast cancer tumor tissues (Asterand). Each core or tumor section was qualitatively scored by a medical pathologist based on the intensity and prevalence of membranous staining: score 0: no staining score; score 1: weak staining in <50% of cells; score 2: intense staining in <50% of cells or weak staining in >50% of cells; score 3: intense staining in >50% of cells. The scores from the 2 cores derived from the same tumor were averaged to generate one score for each tumor.

Analysis of The Cancer Genome Atlas (TCGA)

Cancer gene-expression profiles were obtained using TCGA primary or metastatic sample data through the OmicSoft OncoLand platform, release Q3 2016. The PVR:PVRL2 ratio was performed by dividing the RNA Reads Per Kilobase Million value of PVRL2 by PVR.

Characterization of PVRIG and TIGIT binding interactions and antibody blocking activity

Recombinant PVR Fc or PVRL2 Fc was incubated with PVRIG or TIGIT expressing HEK293 cells for 30 minutes at 4°C and after washing. Bound Fc protein was detected with anti-human IgG secondary antibody. For testing antibody blocking, anti-PVRIG, anti-TIGIT, or relevant isotype control antibody was preincubated with PVRIG HEK293 or TIGIT HEK293 cells, followed by the addition of hPVRL2 or hPVR Fc. After washing, cell-bound hPVRL2 or hPVR Fc was detected. For assessing anti-CD96 activity, recombinant CD96 was adhered onto a 96-well plate, and PVR Fc binding was assessed in the presence of anti-CD96 or isotype control antibody. For assessing anti-PVR and anti-PVRL2 blocking activity, PVR^+PVRL2^+ Expi293 cells were first incubated with anti-PVR, anti-PVRL2, or relevant isotype control antibody, followed by the addition of TIGIT Fc or PVRIG Fc. After washing, cell-bound TIGIT or PVRIG Fc was detected.

In vitro T-cell function assays

$pp65_{(495–503)}$ reactive $CD8^+$ T cells were expanded by culturing $HLA\text{-}A2^+$ PBMCs with 1 μg/mL $pp65_{(495–503)}$ (Anaspec), 2 ng/mL IL2 (R&D Systems), and 10 ng/mL IL7 (R&D Systems). IL2 and IL7 were replenished on days 3 and 5. On day 8, cells were harvested and rested in low-dose IL2 (50 ng/mL). On day 11, cells were phenotyped for $pp65_{(495–503)}$ reactivity by HLA-A*02:01 $pp65_{(495–503)}$ tetramer staining (MBL-BION) and for TIGIT, PVRIG, and CD96 expression. On day 11, cultures contained >90% $pp65_{(495–503)}$ reactive $CD8^+$ T cells. For functional testing, antibodies to PVRIG, CD96, TIGIT, PD-1, PVR, and PVRL2 were added at a final concentration of 10 μg/mL for each antibody. For combination testing, each antibody was tested at 10 μg/mL and, as needed, isotype control antibody concentration was adjusted to match the total antibody concentration. $CD8^+$ T cells were cocultured in a 1:1 ratio in 96-well round-bottom tissue culture plates with Mel-624 or Panc.05.04 cells that have been pulsed with $pp65_{(495–503)}$. After the 18-hour incubation period, conditioned media were analyzed for cytokines using a cytometric bead array (CBA; BD Biosciences). In some experiments, nonadherent cells were harvested after the 18-hour incubation period, and flow cytometry was performed to characterize the expression of PVRIG, TIGIT, PD-1, TIM3, and LAG3. To assess cytotoxic activity, Mel-624 and Panc.05.04 cells were stably transduced with a luciferase

reporter gene (System Biosciences) and used as target cells as described above. After incubation for 18 hours and washing to remove lysed cells, Bio-Glo luciferase substrate (Promega) was added to each well and relative light units (RLU) were qualified on an EnVision multilabel reader (PerkinElmer). The percentage of live cells was calculated by $(RLU_{(\text{target cells + T cells + antibody})}/RLU_{(\text{target cells + T cells + media alone})}) \times 100$.

To assess the effect of checkpoint blockade on human tumor-infiltrating lymphocytes (TILs), human tumors obtained within 24 hours of surgical resection were dissociated (gentleMACS, Miltenyi Biotec), and $CD3^+$ TILs were purified using a $CD3^+$ T-cell isolation kit (Miltenyi Biotec). Isolated $CD3^+$ TILs were cocultured with Mel-624 cells expressing surface bound anti-CD3 scFv at a 10:1 E:T ratio. Antibodies were used at 10 μg/mL final concentration. After 24 to 48 hours, conditioned media were harvested, and cytokine quantities were assessed using a CBA human Th1/Th2/Th17 cytokine kit (BD Biosciences). Data were acquired using a Fortessa flow cytometer (BD Biosciences) and analyzed using FlowJo (Treestar) and Prism GraphPad software.

Results

TIGIT and PVRIG are distinct inhibitory signaling nodes on human $CD8^+$ T cells

To identify additional immune checkpoints, we developed predictive computational algorithms based on shared genomic and proteomic characteristic among known immune-checkpoint receptors, such as gene structure, protein domains, predicted cellular localization, and expression patterns. Using these algorithms, we identified PVRIG as an immune receptor in the nectin family. The relevance of PVRIG in relation to other receptors of the nectin family (e.g., TIGIT, CD96) in regulating $CD8^+$ T-cell responses has not been reported. To compare the effects of PVRIG, TIGIT, and CD96 blockade, we generated or identified antibodies that disrupt the interaction of each receptor with their respective cognate ligand. For PVRIG, we generated a high-affinity, humanized anti-PVRIG, COM701, which blocks the interaction of PVRIG with PVRL2 (Fig. 1A; Supplementary Fig. S1). For TIGIT and CD96, anti-TIGIT (Fig. 1B) and anti-CD96 (Fig. 1C) were identified that block the binding of PVR to these receptors. The effect of blocking these receptors was examined on human $CD8^+$ effector T cells. PBMCs activated with a viral antigen peptide ($pp65_{(495–503)}$), IL2, and IL7 for 11 days expressed PVRIG, TIGIT, and CD96 on $pp65_{(495–503)}$ specific $CD8^+$ T cells. Coexpression of PVRIG with TIGIT was observed (Supplementary Fig. S2A), with TIGIT expression peaking early (day 3) and PVRIG and CD96 expression peaking later (day 11; Fig. 1D; Supplementary Fig. S2B). Day 11 activated pp65-specific $CD8^+$ T cells were cocultured with $pp65_{(495–503)}$ pulsed Mel-624 or Panc.05.04 cancer cell lines that express PVR and PVRL2 (Fig. 1E). PVRIG or TIGIT blockade increased cytokine production, whereas CD96 blockade with 2 distinct antibodies had no effect (Fig. 1F; Supplementary Fig. S2C). As these are primary human T cells, variability was observed, but the magnitude of effect of PVRIG blockade was related to the amount of PVRIG expression (Supplementary Fig. S2D). The combination of PVRIG and TIGIT blockade enhanced IFNγ production, whereas combinations with CD96 blockade did not increase IFNγ compared with single-agent treatments (Fig. 1G). Assessing the effects on multiple donors, we observed that anti-PVRIG, anti-TIGIT, and the combination of anti-PVRIG and anti-TIGIT significantly increased IFNγ (Fig. 1H). The majority of donors had at least an additive effect from PVRIG and TIGIT blockade, with synergistic combination activity (depicted in filled symbols) observed in some donors (Fig. 1H). Similar changes in TNFα were also observed (Supplementary Fig. S2E). Although DNAM-1 was expressed on $pp65_{(495–503)}$ specific effector T cells (Supplementary Fig. S2F), anti-DNAM-1 had no effects on IFNγ secretion (Supplementary Fig. S2G and S2H), indicating that this T-cell restimulation assay system was not dependent on DNAM-1 signaling. To determine whether changes in T-cell function by anti-PVRIG could be caused by antibody-mediated dimerization independent of PVRL2, T cells were activated in a PVRL2-independent assay with plate-bound anti-CD3 and anti-PVRIG. No changes in T-cell activation were observed with plate-bound anti-PVRIG compared with plate-bound IgG (Supplementary Fig. S2I). In addition to changes in cytokine production, PVRIG and TIGIT blockade also increased cytotoxic function of $CD8^+$ T cells (Fig. 1I). These data demonstrate an inhibitory role for PVRIG and TIGIT in regulating $CD8^+$ effector T-cell function.

Although TIGIT is reported to bind to PVR and PVRL2 (15), the affinity of TIGIT to PVRL2 is weak (6 μmol/L) (24). We were not able to observe an interaction between TIGIT and PVRL2 by surface plasmon resonance or ELISA (Supplementary Fig. S3A). In contrast, the affinity of PVRIG to PVRL2 is reported to be 88 nmol/L (13), indicating that PVRIG is a high-affinity receptor for PVRL2. To demonstrate that PVRIG–PVRL2 interactions represent a distinct signaling node from TIGIT–PVR, we identified neutralizing antibodies to PVR and PVRL2, based on blocking the interaction of PVR with TIGIT and PVRL2 with PVRIG (Fig. 2A and B). Anti-PVR and anti-PVRL2 increased IFNγ production by $CD8^+$ T cells (Fig. 2C; Supplementary Fig. S3B). Combination of PVR blockade with TIGIT blockade did not further increase IFNγ production, suggesting that TIGIT and PVR are overlapping pathways. In contrast, coblockade of TIGIT and PVRL2 increased IFNγ production, indicating that TIGIT and PVRL2 are nonoverlapping signaling nodes (Fig. 2C; Supplementary Fig. S3B). We examined the effects of anti-PVRIG with anti-PVR or anti-PVRL2 and observed that PVRIG and PVR blockade, but not PVRIG and PVRL2 blockade, resulted in an increase in IFNγ as compared with single antibody blockade (Fig. 2C; Supplementary Fig. S3B). When we compared the combination of receptor blockade (i.e., anti-PVRIG and anti-TIGIT) with the combination of ligand blockade (i.e., anti-PVR and anti-PVRL2), similar increases in IFNγ were observed (Fig. 2D), suggesting no additional functional interactions are present among these proteins. Taken together, these data show that PVRIG is the dominant inhibitory receptor for PVRL2. These data place PVRIG-PVRL2 and TIGIT–PVR as two nonredundant, juxtaposed inhibitory signaling nodes.

As PD-1 is an inhibitory receptor on $CD8^+$ T cells, we examined the effects of combinatorial blockade of PVRIG, TIGIT, and PD-1. Activated $pp65_{(495–503)}$ specific $CD8^+$ T cells expressed PD-1 and Panc.05.04 cells expressed PD-L1 (Fig. 2E). We next performed a coculture of the $pp65_{(495–503)}$ reactive $CD8^+$ T cells with $pp65_{(495–503)}$ pulsed Panc.05.04 cells in the presence of blocking antibodies to PVRIG, TIGIT, and/or PD-1. In comparison with PD-1, PVRIG blockade resulted in a comparable increase in IFNγ (Fig. 2F). Although anti-PVRIG and anti–PD-1 also led to additive increases in IFNγ production as compared with each individual antibody, the combination of anti-PVRIG with

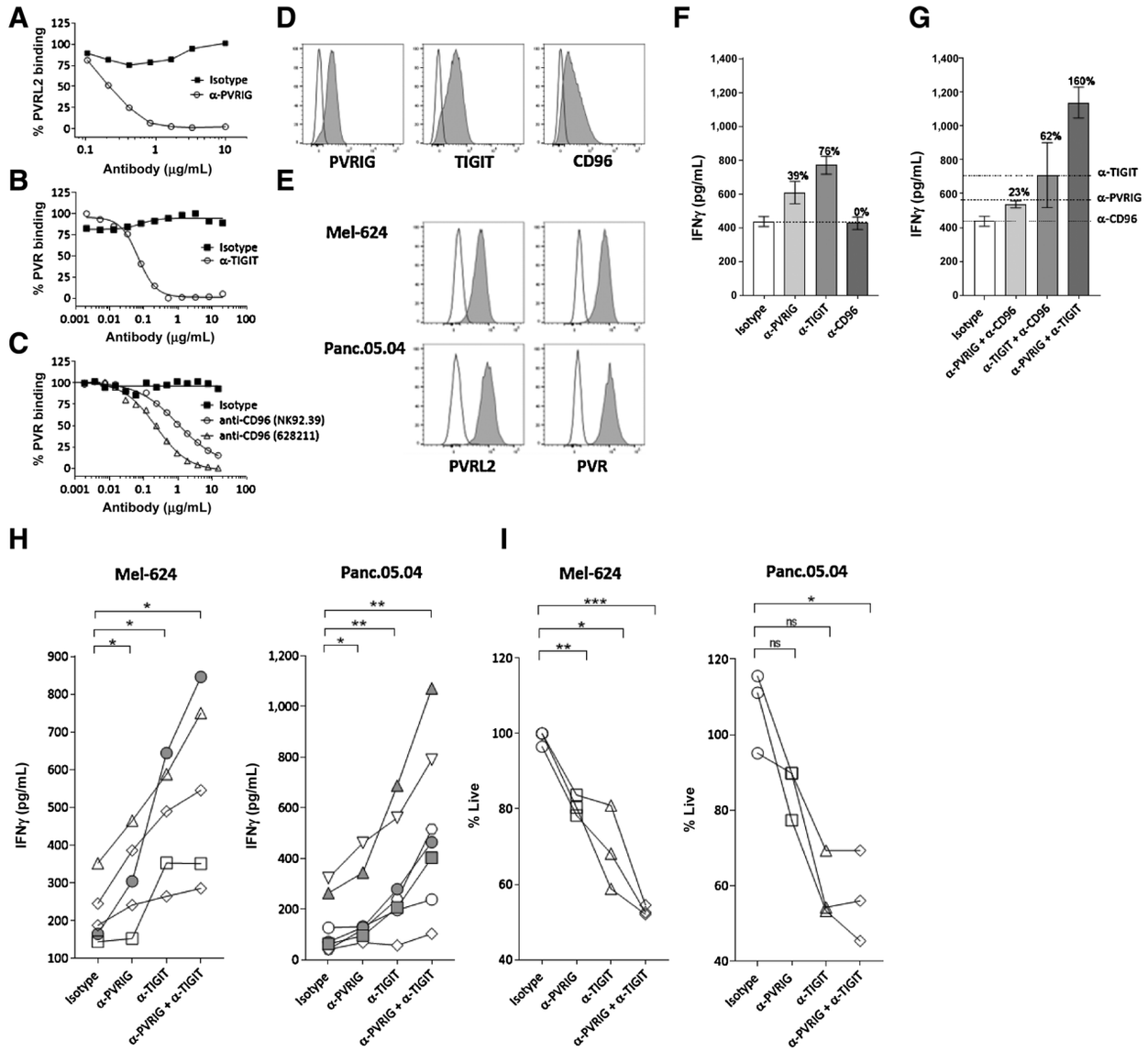

Figure 1.

PVRIG and TIGIT, but not CD96, are inhibitory receptors on CD8$^+$ T cells. **A,** The effect of anti-PVRIG on blocking the binding of PVRL2 Fc to PVRIG expressing HEK293 cells is depicted. **B,** Binding of PVR Fc to TIGIT expressing HEK293 cells in the presence of anti-TIGIT or isotype control is shown. **C,** The effect of anti-CD96 in disrupting the binding of PVR Fc to CD96 HIS recombinant protein is shown. **D,** Expression of PVRIG, TIGIT, and CD96 (filled) relative to IgG (line) on pp65$_{(495–503)}$ specific CD8$^+$ T cells on day 11 is shown. **E,** PVR and PVRL2 expression on Mel-624 and Panc.05.04 tumor cells is depicted. **F–I,** Day 11 activated pp65$_{(495–503)}$ specific CD8$^+$ T cells from 5 to 7 donors were cocultured for 18 hours with pp65$_{(495–503)}$ peptide–pulsed Mel-624 cells and anti-PVRIG, anti-TIGIT, anti-CD96, or isotype control either alone (**F**) or in combination (**G**). IFNγ production and cytotoxic activity were assessed. **F, G,** A representative donor of the 5 to 7 donors evaluated is shown. In **F** and **G**, average + SD is shown of 3 replicate wells. The percentage of change for each condition relative to isotype control is depicted above each bar. In **G**, the dashed line represents the amount of IFNγ present in single antibody treatment conditions. **H,** Each line represents an individual donor of a total of 5 to 7 donors tested. **I,** Cytotoxic activity of each antibody relative to vehicle was calculated, and the percentage of live cells after antibody treatment is shown. For **H, I,** data were analyzed by paired Student t test; *, $P < 0.05$; **, $P < 0.01$; ***, $P < 0.001$. Data are representative of at least 2 to 3 experiments for each donor. Additional statistical analyses are shown in Supplementary Fig. S7A.

anti-TIGIT had a greater effect on T-cell activation than the combination with PD-1 blockade (Fig. 2F). Triple combination of PVRIG, TIGIT, and PD-1 blockade resulted in the greatest increase in IFNγ (Fig. 2F; Supplementary Fig. S3C). These data provide a rationale for dual blockade of PVRIG with TIGIT or PD-1 blockade, and triple blockade of PVRIG, TIGIT, and PD-1, to enhance CD8$^+$ effector function.

Blockade of the PVRIG–PVRL2 interaction induces PD-1 and TIGIT expression

To gain mechanistic insight into how different inhibitory checkpoint receptors can be coregulated, we next evaluated whether PVRIG blockade modulated expression of other inhibitory receptors. Blockade of PVRIG led to induction of TIGIT expression (Fig. 3A) but did not modulate LAG-3 or TIM3

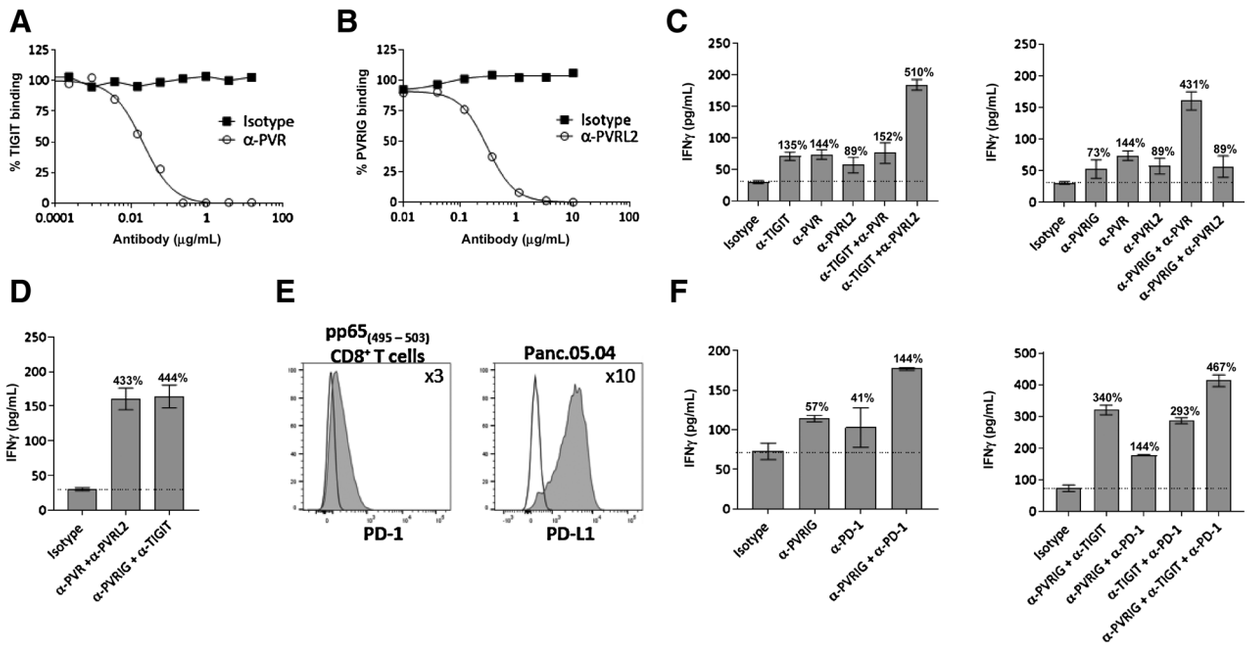

Figure 2.

TIGIT–PVR and PVRIG–PVRL2 are distinct inhibitory pathways. **A,** The effect of anti-PVR antibody in blocking the binding of TIGIT Fc to PVR$^+$ Expi293 cells is shown. **B,** Anti-PVRL2 blocked the binding of PVRIG Fc to PVRL2$^+$ Expi293 cells. **C** and **D,** Day 11 activated pp65$_{(495–503)}$ specific T cells were cocultured for 18 hours with pp65$_{(495–503)}$ peptide–loaded Mel-624 cells and anti-PVRIG, anti-TIGIT, anti-PVR, anti-PVRL2, or isotype control either alone or in combination. IFNγ production is depicted. **E,** Expression of PD-1 (shaded) on activated pp65$_{(495–503)}$ CD8$^+$–specific T cells and expression of PD-L1 (shaded) on Panc.05.04 cells relative to IgG (line) are shown. **F,** pp65$_{(495–503)}$ specific CD8$^+$ T cells were cocultured for 18 hours with pp65$_{(495–503)}$ pulsed Panc.05.04 and anti-PVRIG, anti-TIGIT, anti–PD-1, or isotype control either alone or in combination. IFNγ production is depicted. Average + SD of 3 replicate wells for a donor is shown and are representative of at least 3 experiments. The percentage of change in IFNγ relative to isotype control is depicted by the number above each bar. Additional data for other donors tested with conditions from Supplementary Fig. S3B–S3C.

expression (Supplementary Fig. S3D and S3E). A small change in PD-1 expression was observed with PVRIG inhibition (Supplementary Fig. S3F). These data suggest that PVRIG blockade induced an increase in TIGIT expression that was not a result of overall enhanced T-cell activation. In contrast to the induction of inhibitory receptors seen with PVRIG blockade, we observed no changes in PVRIG expression after TIGIT or PD-1 blockade as compared with treatment with isotype control (Supplementary Fig. S3G). We also assessed expression of PVRIG on T cells after coculture with tumor cells alone, or with TIGIT or PD-1 blockade. In the absence of antibody treatment, coculture of CD8$^+$ T cells with target cells alone resulted in reduced surface expression of PVRIG but not TIGIT as compared with prior to coculture (Fig. 3B). As other checkpoint receptors such as

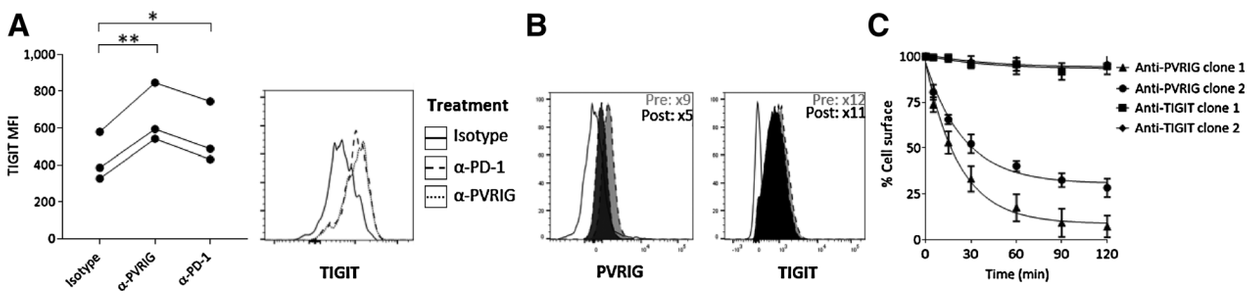

Figure 3.

PVRIG antagonism results in increased TIGIT expression. **A,** pp65$_{(495–503)}$ pulsed Panc.05.04 were cocultured with pp65$_{(495–503)}$ specific CD8$^+$ T cells from 3 donors and the indicated antibodies. After 18 hours, nonadherent cells were assessed for TIGIT expression on pp65$_{(495–503)}$ specific CD8$^+$ T cells and depicted for 3 donors. A representative histogram gated on pp65$_{(495–503)}$ specific CD8$^+$ T cells is shown. The solid line represents isotype control mAb, dotted line represents anti-PVRIG, and dashed line represents anti–PD-1. *, $P < 0.05$; **, $P < 0.01$. **B,** Expression of PVRIG and TIGIT on pp65$_{(495–503)}$ CD8$^+$ T cells was assessed before and 18 hours after coculture with the pp65$_{(495–503)}$ pulsed Panc.05.04 tumor cell line. **C,** Internalization of PVRIG and TIGIT was assessed at multiple time points using 2 antibodies each. A representative donor of 3 donors evaluated is shown. Data are representative of at least 2 experiments for each donor.

CTLA-4 undergo rapid internalization as a mechanism to regulate functional activity (25, 26), we assessed internalization of PVRIG and TIGIT on activated T cells to determine if the above observations could be due to internalization. Using anti-PVRIG antibodies of different epitope bins (Supplementary Fig. S3H), we observed that cell-surface PVRIG appears to be rapidly internalized upon culturing cells at 37°C, with more than 50% of the cell-surface PVRIG being internalized within 60 to 120 minutes (Fig. 3C). In contrast, TIGIT remained on the cell surface, with less than 20% internalized at 2 hours at 37°C (Fig. 3C). These data hint at complex mechanisms regulating PVRIG expression.

PVRIG expression is induced in human tumors and coexpressed with PD-1 and TIGIT

We next examined the expression of PVRIG and TIGIT on immune cells from blood and tumor tissue. In the peripheral blood of healthy donors, we observed that PVRIG and TIGIT were the highest on memory cell populations (Supplementary Fig. S4A). To examine the expression of PVRIG on TILs, human tumors were dissociated and stained for members of the PVRIG and TIGIT axis. Positive expression of PVRIG was detected on $CD8^+$ and $CD4^+$ T cells (Fig. 4A), and NK cells (Supplementary Fig. S4B) from all tumor types were examined. Ovarian, kidney, lung, endometrial, and breast cancers demonstrated the highest PVRIG expression on $CD4^+$ and $CD8^+$ T cells, with some donors in these cancers displaying greater than 10-fold PVRIG expression relative to isotype. In addition to these cancer types, PVRIG was also highly expressed on NK cells from prostate cancer (Supplementary Fig. S4B). For lung tumors, we were able to obtain normal adjacent tissue (NAT) from the same patient from several donors. In this cohort, PVRIG expression on $CD4^+$ and $CD8^+$ TILs was significantly higher compared with T cells isolated from matching NAT (Fig. 4B). Furthermore, we examined whether PVRIG, TIGIT, or PD-1 expression associated with an exhausted or effector phenotype by examining expression of Eomes and T-bet, transcription factors that regulate $CD8^+$ T-cell function. In contrast to TIGIT or PD-1, PVRIG expression on $CD8^+$ TILs significantly correlated with an $Eomes^+T\text{-}bet^-$ phenotype, indicating induction of PVRIG expression on exhausted T cells (Fig. 4C; Supplementary Fig. S4C). The presence of intracellular PVRIG was detected on $CD8^+$ TILs after permeabilization, but the majority of PVRIG was detected on the cell surface (Supplementary Fig. S4D–S4F). Activation with anti-CD3 and anti-CD28 was carried out with 3 tumor samples in which PVRIG expression was low or not present *ex vivo*. Activation enhanced the expression of PVRIG, suggesting that PVRIG expression can be induced if TILs are reactivated (Supplementary Fig. S4G). As coblockade of PVRIG, TIGIT, and PD-1 resulted in synergistic effects on T-cell function for some donors, we examined the coregulation of PVRIG, TIGIT, and PD-1 on T-cell populations. PVRIG was coexpressed with TIGIT and PD-1 on $CD4^+$ and $CD8^+$ T cells, and with TIGIT on NK cells (Fig. 4D). Furthermore, a positive correlation was observed between PVRIG expression and PD-1 or TIGIT expression on $CD4^+$ TILS (Fig. 4E). For $CD8^+$ T cells, cells that expressed higher PVRIG also generally expressed higher PD-1 and TIGIT. Taken together, these data demonstrate that PVRIG is expressed on T cells and NK cells from multiple human cancers, with the $PVRIG^+$ cells being associated with an exhausted molecular phenotype on $CD8^+$ T cells.

PVRL2 expression is enhanced in tumor tissue compared with NAT

We next examined whether PVRL2 expression was induced in human cancers and was concomitant with PVRIG expression in human cancer tissues. On multiple tumor types, expression of PVRL2 was observed on $CD45^-$ cells (Fig. 5A), likely composed of tumor epithelial cells and other nonimmune cells, and on $CD14^+$ cells (Fig. 5B), likely composed of monocytes and tumor-associated macrophages (TAM). No expression of PVRL2 was detected on lymphocytes (13). Of the cancers examined, endometrial, lung, ovarian, and breast cancers had high expression of PVRL2 on both $CD14^+$ and $CD45^-$ cells. These are potential indications where targeting PVRIG alone or in combination with TIGIT or PD-1 inhibitors may have clinical benefit. In lung cancer, PVRL2 expression was significantly induced on TAMs. On $CD45^-$ cells, PVRL2 expression was increased in 5 of 7 tumor samples as compared with matched NAT (Fig. 5C), but this effect was not statistically significant. Within the same tumor sample, coexpression of PVRIG on $CD8^+$ T cells and PVRL2 on TAMs and $CD45^-$ cells were observed in the same tumor sample, suggesting that this pathway can be coexpressed in the same tumor (Fig. 5D).

Our *in vitro* data demonstrate that PVRIG–PVRL2 and TIGIT–PVR interactions provide nonredundant inhibitory signals to T cells. Based on this, tumors with high PVRL2 expression and lower PVR expression are more likely to respond to PVRIG blockade as compared with TIGIT blockade. To determine whether any cancer types were higher for PVRL2 compared with PVR, we examined RNA transcript data to assess the relative expression of PVR to PVRL2 in primary human tumors. We noted that breast, ovarian, prostate, and endometrial cancers were among the cancers with the highest ratio of PVRL2 to PVR (Fig. 5E), suggesting these are cancer types in which PVRL2 might prominently regulate the immune response. In contrast, melanoma, esophageal, and colorectal cancers had higher expression of PVR relative to PVRL2. We further examined protein expression of PVR and PVRL2 by flow cytometry on dissociated tumors. PVR^+PVRL2^+ $CD45^-Epcam^+$ cells were observed in the majority of tumor samples examined, with endometrial cancers having the highest percentage of PVR^+PVRL2^+ cells (Fig. 5F). In alignment with the RNA transcript analysis, we observed a high percentage of PVR^-PVRL2^+ tumor cells in ovarian, prostate, and endometrial cancers, whereas colorectal and kidney cancer samples had high percentages of PVR^+PVRL2^- tumor cells (Fig. 5F). These data suggest that the relative dominance of PVRIG–PVRL2 and TIGIT–PVR pathways was dependent on the tumor type, and thus highlight the need to characterize the expression profile of each pathway to select the suitable single-agent or combination treatment.

Detection of PD-L1 on patient tumors with IHC is currently the most common clinically validated biomarker for predicting patient response to anti–PD-1/PD-L1 therapy (27–29). We also examined the expression of PVRL2 in tumor samples by IHC in an independent cohort of breast, colon, lung, ovarian, kidney, and skin cancers. An FFPE compatible and specific anti-PVRL2 was identified by staining FFPE-embedded cell line pellets and Western blots of cell lysates (Supplementary Fig. S5). In comparison with normal tissue, PVRL2 expression was induced in ovarian, breast, lung, kidney, and colon cancers (Table 1; Fig. 5G). Of the 6 tumor types examined, breast, ovarian, and lung cancers had the

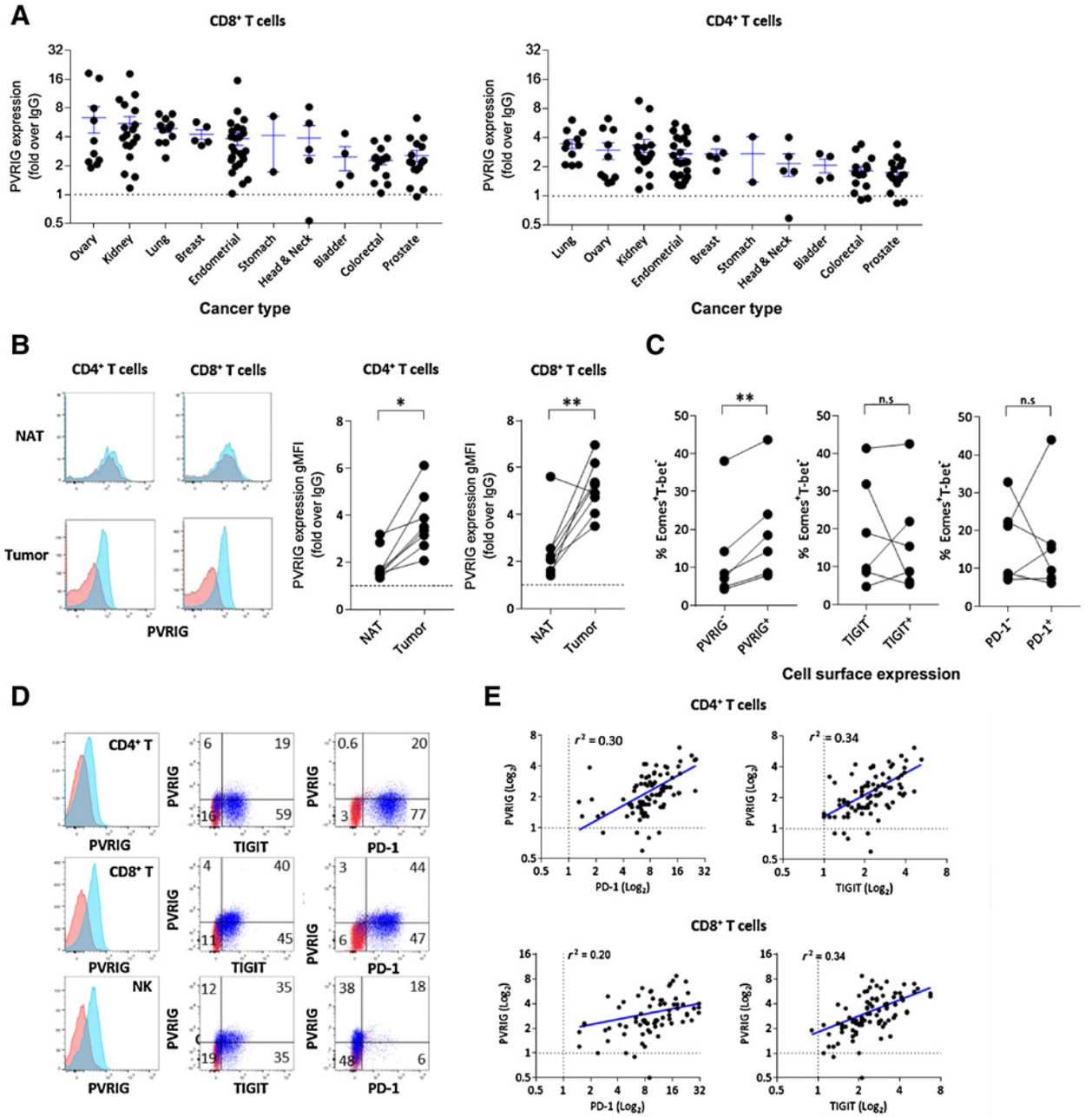

Figure 4.

PVRIG is induced on tumor-infiltrating lymphocytes. **A,** Expression of PVRIG on CD8$^+$ and CD4$^+$ TILs from dissociated human tumors of various cancer types is shown. Each dot represents a distinct tumor from an individual patient. Average + SEM is shown by the ticks. Dotted line represents no staining. **B,** Expression of PVRIG on CD4$^+$ and CD8$^+$ T cells from donor-matched lung NAT and lung cancer is shown. Red is staining with isotype control, and blue is staining for PVRIG, TIGIT, or PD-1. **C,** Three ovarian and three endometrial tumors were dissociated and stained for cell-surface PVRIG, TIGIT, PD-1, and CD8, followed by intracellular staining for Eomes and T-bet. The percentage of Eomes$^+$T-bet$^-$ cells within PVRIG$^\pm$, TIGIT$^\pm$, and PD-1$^\pm$ cell subsets is shown. For **B** and **C**, a paired Student *t* test was performed, *, $P < 0.05$; **, $P < 0.01$. **D,** Representative flow cytometry plots depicting the coexpression of PVRIG, TIGIT, and PD-1 on CD4$^+$, CD8$^+$, and NK TILs from endometrial cancer sample are shown. **E,** For all dissociated tumor samples analyzed, PVRIG expression was plotted versus PD-1 and TIGIT expression on CD4$^+$ and CD8$^+$ T cells. A Pearson correlation analysis was performed, and r^2 values were shown.

highest incidence of strong PVRL2 expression (Table 1). We observed that PVRL2 was primarily expressed on tumor cells but was also detected in some samples on immune cells (Supplementary Fig. S5G). PVRL2 expression was detected on both PD-L1$^+$ and PD-L1$^-$ tumors (Supplementary Fig. S6A) and was not induced by IFNγ (Supplementary Fig. S6B). These data, along with our studies analyzing dissociated tumors, provide orthogonal confirmation of high expression of PVRL2 in breast, ovarian,

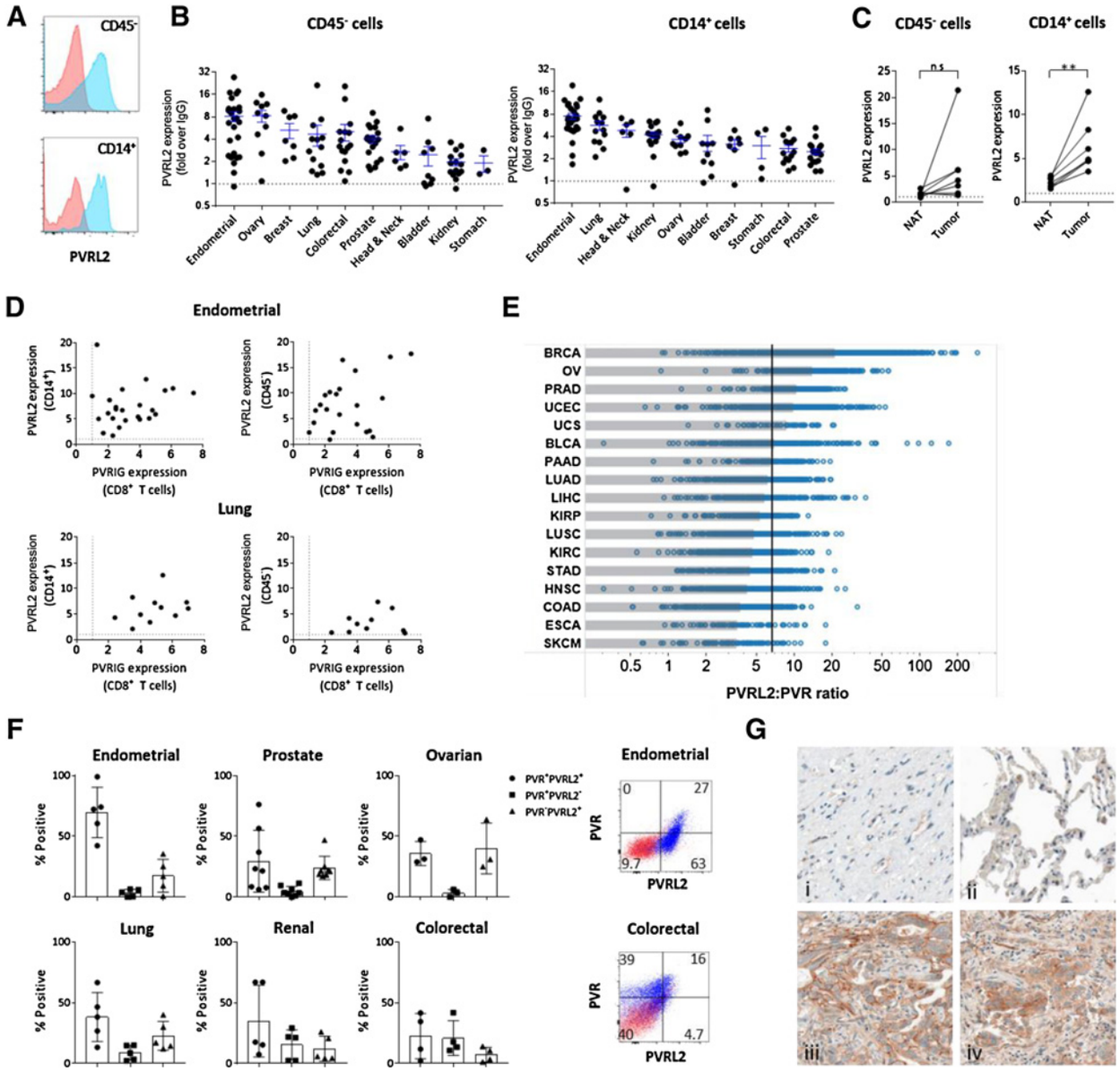

Figure 5.

PVRL2 expression is increased in the TME. **A,** PVRL2(blue) expression relative to IgG (red) on CD45$^-$ and CD14$^+$ cells from a lung tumor is shown. **B,** PVRL2 expression from dissociated tumors determined by flow cytometry on (**A**) CD45$^-$ cell and (**B**) CD14$^+$ TAM subsets is shown, with each dot being an individual dissociated tumor sample for each tumor type. Average + SEM is shown for each cancer type. Dotted line represents no staining. **C,** Expression of PVRL2 on CD14$^+$ cells and CD45$^-$ cells from donor matched lung NAT and lung cancer is shown. A paired Student *t* test was performed. **, $P < 0.01$. **D,** Coexpression of PVRIG on CD8$^+$ T cells and PVRL2 expression on CD14$^+$ and CD45$^-$ cells for endometrial and lung cancer samples are shown. Each dot represents an individual tumor sample. **E,** The ratio of the PVRL2-to-PVR RNA transcript was calculated, and tumor types were plotted from highest (top) to lowest (bottom). For each cancer type, the median is represented by the gray box. The black line represents the median value of all samples. Abbreviations are based on TCGA nomenclature. **F,** In dissociated tumor samples, the coexpression of PVR and PVRL2 was assessed by flow cytometry on CD45$^-$Epcam$^+$ tumor epithelial cells. Representative PVR or PVRL2 expression (blue) relative to isotype control (red) for ovarian and endometrial cancer is shown. **G,** Representative PVRL2 staining in normal ovary tissue (i), normal lung tissue (ii), ovarian tumor (iii), and lung tumor (iv) is shown. Magnification, ×40.

and lung cancers and suggest that the PVRIG–PVRL2 pathway may inhibit T-cell activity in PD-L1$^-$ tumors.

To demonstrate an effect of blocking these pathways on tumor immunity, we assessed the single and combinatorial effect of anti–PD-1, anti-PVRIG, and anti-TIGIT on CD3$^+$ TILs from patients of different cancer indications, namely, endometrial, ovarian, kidney, head and neck, and lung. In these experiments, TILs were isolated from human tumors and directly *ex vivo* cocultured with Mel-624 cells engineered to express a membrane bound anti-CD3 scFv (Mel-624 OKT3). Anti-CD3 scFv was

Table 1. Expression of PVRL2 in human tumors

	PVRL2^{+}, [b]	Total examined	% PVRL2^{+}, [b]	% PVRL2^{high}, [c]
Ovarian				
Normal	0	2	0	0
High-grade serous carcinoma	8	12	67	42
Mucinous carcinoma	4	6	67	33
Endometrioid carcinoma	8	12	67	25
Breast				
Normal	0	4	0	0
Invasive ductal carcinoma	19	30	63	46
Triple-negative ductal carcinoma[a]	28	30	93	46
Lung				
Normal	1	4	25	25
Adenocarcinoma	8	14	57	29
Squamous cell carcinoma	8	13	62	33
Renal				
Normal	0	3	0	0
Clear cell carcinoma	8	20	40	15
Papillary renal cell carcinoma	2	7	29	29
Colon				
Normal	0	2	0	0
Adenocarcinoma	16	30	53	7
Skin				
Normal	0	4	0	0
Melanoma: primary	3	24	13	0
Melanoma: metastatic	1	12	8	0

[a]Assessed using full-face tumor sections.
[b]Positive staining defined by score > 1.
[c]High expression defined by score > 2.

utilized as a surrogate method of T-cell activation in the absence of defined antigen specificity of these human TILs. To avoid further manipulation of TILs *ex vivo*, no additional expansion of TILs by IL2 or other methods was performed prior to coculture. T cells cultured with Mel-624 OKT3 produced more cytokines than the T cells alone or when cocultured with Mel-624 parental cells, indicating that an anti-CD3 scFv on the cell surface was activating T cells (Supplementary Fig. S6C). As expected for cancer patient–derived TILs, donor-to-donor variability in the amount of cytokine produced was observed. In 5 of 10 tumor samples examined, IFNγ production by purified TILs was increased by anti-PVRIG, similar in potency to anti-TIGIT or anti–PD-1 (Fig. 6A). When anti-PVRIG was combined with anti-TIGIT antibody, a statistically significant increase in IFNγ relative to isotype control was observed, and this combination was more potent than anti–PD-1 alone (Fig. 6B). Representative examples of minimal single-agent activity with anti-PVRIG or anti-TIGIT, but synergistic activity in combination are shown (Fig. 6C–F). These data provide a rationale for dual blockade of PVRIG and TIGIT or of PVRIG and PD-1 to enhance CD8^{+} T-cell effector function. For a lung cancer sample, we were able to isolate sufficient T cells to examine additional combinations and observed that anti-PVRIG or anti-TIGIT with an anti–PD-1 also resulted in further increases of IFNγ and IL2 compared with single agent. In this donor, the triple blockade of PVRIG, TIGIT, and PD-1 did not further increase IFNγ or IL2. Taken together, we demonstrate an activation effect of blocking PVRIG, TIGIT, and PD-1 on freshly isolated CD3^{+} TILs from human cancers.

Discussion

PVRIG is a member of the nectin and nectin-like family, which includes several known immunoregulatory receptors. Examining the interplay of the receptors within this family is crucial to understanding the relevance of each receptor. Here, we elucidated the activity of these receptors using antagonistic antibodies to TIGIT, CD96, PVRIG, PVR, and PVRL2. Our studies show that PVRIG and TIGIT are inhibitory receptors on effector T cells, suppressing cytokine production and cytotoxic activity. Although CD96 was reported to be inhibitory on mouse NK cells (20), our data using two anti-CD96 clones and data from others demonstrate that human CD96 does not suppress lymphocyte function (21). CD96 may well regulate other aspects of T-cell function. We further demonstrate that TIGIT and PVRIG are nonoverlapping pathways, with TIGIT signaling being activated by PVR and PVRIG signaling being activated by PVRL2. Although PVRIG and TIGIT expression are both induced upon T-cell activation, PVRIG expression is unique in several aspects, correlating with Eomes^{+}T-bet^{-} expression on TILs and rapidly internalizing from the cell surface in the absence of TCR signaling. As rapid internalization of CTLA-4 is believed to regulate the function of CTLA-4 (30), the internalization of PVRIG may constitute a similar regulatory mechanism. PVRIG blockade as a single agent was sufficient to increase cytokine production and cytotoxic activity by CD8^{+} effector T cells, including *ex vivo*–isolated TILs. Furthermore, PVRIG deficiency in mice resulted in increased CD8^{+} T-cell responses and reduced tumor growth *in vivo* (31). Taken together, the functional data demonstrate single-agent activity for PVRIG blockade in regulating effector T-cell function and indicate a role for PVRIG in regulating effector T-cell function in cancer.

PVRIG blockade in combination with TIGIT blockade enhanced cytokine production and cytotoxic function, providing a rationale for combination therapies using PVRIG antagonism. These data, along with previous studies demonstrating a role for PVRIG and TIGIT in regulating dendritic cell–T-cell interactions and NK cell–tumor cell interactions (13, 22), provide several mechanisms by which blocking these pathways can enhance antitumor immune response. Combination of PVRIG

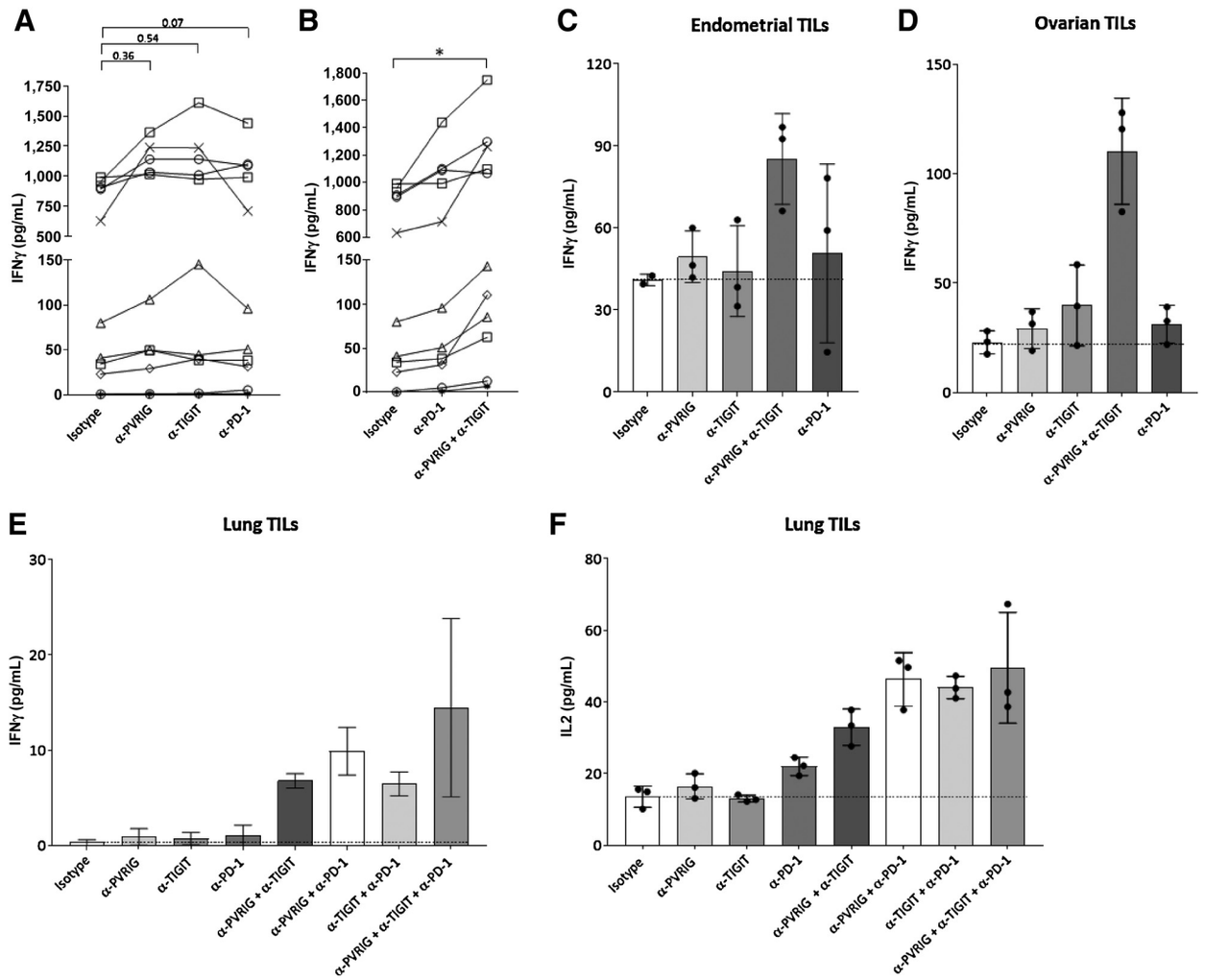

Figure 6.

PVRIG and TIGIT blockade on human TILs stimulated *ex vivo*. Freshly isolated CD3$^+$ TILs from tumors obtained within 24 hours of surgical resection were cultured with Mel-624 OKT3, a modified Mel-624 tumor cell line expressing surface-bound anti-CD3 scFv (OKT3). Anti-PD IFNγ amounts in the presence of (**A**) anti-PVRIG, anti-TIGIT, anti–PD-1, or isotype control or with (**B**) anti–PD-1, anti-PVRIG and anti-TIGIT, or isotype control were assessed. *, $P < 0.05$ (paired Student *t* test). Each individual mark represents a different tumor sample donor. **C–F,** Representative IFNγ or IL2 production after checkpoint blockade in endometrial (**C**), ovarian (**D**), and lung (**E, F**) TILs is shown. For **C–F,** each dot is a technical replicate and average + SD are depicted by bar and tick marks. Additional statistics are shown in Supplementary Fig. S7D and S7E.

and PD-1 blockade also increased cytokine production by human T cells. We observed that PVRIG was coexpressed with PD-1 and TIGIT at the single-cell level on TILs, peripheral memory T cells, and activated T cells, and that cells with higher PVRIG expression generally had higher TIGIT and PD-1 expression. These data indicate that the overall contribution of these 3 inhibitory receptors may regulate the antitumor response. Supporting this, the triple combination of PD-1 antibody with PVRIG or TIGIT inhibitors resulted in the greatest increase in T-cell function.

We report here on a high-affinity anti-human PVRIG antibody, COM701, which disrupts the interaction of PVRIG and PVRL2. To determine cancer indications that could refine patient selection for clinical trials, we examined the expression profile of this axis in human cancers. For PVRIG, we observed that expression of PVRIG on T cells was highest in ovarian, lung, breast, endometrial, and kidney cancers. Considering that PVRIG is induced upon T-cell activation and given that the majority of TILs are antigen experienced (32, 33), the extent of T-cell activation, rather than the tissue in which the tumor is located or originated, likely determines expression of PVRIG on TILs. This is consistent with the observation that PVRIG and PD-1 expression was coexpressed. As expression of PD-L1 has been correlated with clinical response to PD-1 inhibitors in several but not all studies (27–29, 34), we also analyzed PVRL2 expression and observed that PVRL2 expression is greater in cancer relative to normal tissues, with highest expression in breast, endometrial, lung, and ovarian cancers. High expression of PVRL2 in breast and ovarian cancers was previously reported (35). We further compared the expression of PVRL2 with PVR and noted that all samples examined contain tumor cells that coexpress PVR and PVRL2, indicating the need for combination

therapy to eliminate these cells. In addition, the relative expression of PVR and PVRL2 was dependent on cancer type. Based on analysis of RNA transcripts, we observed that breast, ovarian, prostate, and endometrial cancers were enriched in PVRL2 expression, whereas melanoma, esophageal, and colorectal cancers were enriched in PVR expression. Analysis of protein expression of PVR and PVRL2 using dissociated tumors confirmed these findings. The presence of PVR^+PVRL2^+, PVR^+PVRL2^-, and PVR^-PVRL2^+ tumor cells further suggests the value of combining TIGIT and PVRIG blockade to alleviate suppressive mechanisms within a heterogeneous TME.

We also compared the expression of PVR and PVRL2 with PD-L1 expression to identify specific cancer types in which the PVRIG–PVRL2 pathway could be a checkpoint. Our data demonstrate that PVRL2 expression was not correlated with PD-L1 or induced by IFNγ. PVRL2 expression on epithelial cells is induced during tumorigenesis, as well as in response to stress and DNA damage (36, 37). PVR and PVRL2 may suppress immune responses independently of PD-L1, and therefore inhibitors of PVRIG and TIGIT could be critical in patients who are PD-L1 negative or who do not respond to or progress with PD-1 inhibitors. Although PD-L1 expression is correlated with TIL infiltration, a subset of melanoma (38) and non–small cell lung cancer tumors (39) are infiltrated with T cells but have low PD-L1 expression. In these patients, the antitumor T-cell response may be mediated by other inhibitory receptors such as PVRIG and/or TIGIT. In support of this, our data using the combination of PVRIG and TIGIT blockade show similar or better activity than PD-1 blockade.

In summary, we characterized the expression of the PVRIG–PVRL2 axis in human cancers and demonstrated a role for PVRIG and TIGIT in regulating the interaction between $CD8^+$ T cells and tumor cells. These data extend our current understanding of PVRIG biology and provide a rationale for clinical testing of COM701, an antibody to PVRIG, in patients with cancer.

Disclosure of Potential Conflicts of Interest

S. Liang, S. Whelan, and K. Hansen have ownership interest in Compugen. J. Taube reports receiving commercial research funding from Bristol-Myers Squibb and is a consultant/advisory board member for Bristol-Myers Squibb, AstraZeneca, Merck, and Amgen. A.N. Fader has received speaker bureau honoraria from Merck. M. White is Sr. Director Antibody R&D at and has ownership interests in Compugen. D.M. Pardoll reports receiving commercial research funding from Bristol-Myers Squibb, Compugen, and AstraZeneca; has ownership interest in Aduro Biotech, DNAtrix, Dracen, Ervaxx, Five Prime Therapeutics, Potenza, Tizona, Trieza, and WindMil; and is a consultant/advisory board member for Amgen, Bayer, FLX Bio, Immunomic, Janssen, Merck, Rock Springs Capitol, and Tizona. No potential conflicts of interest were disclosed by the other authors.

Authors' Contributions

Conception and design: E. Ophir, O. Levy, S. Kumar, L. Dassa, I.-M. Shih, M. White, D.M. Pardoll, S.C. Liang
Development of methodology: S. Whelan, E. Ophir, S. Ganguly, L. Leung, I. Vaknin, S. Kumar, L. Dassa, A.N. Fader, D.M. Pardoll, S.C. Liang
Acquisition of data (provided animals, acquired and managed patients, provided facilities, etc.): S. Whelan, M.F. Kotturi, S. Ganguly, L. Leung, S. Kumar, K. Hansen, D. Bernados, B. Murter, A.N. Fader, S.C. Liang
Analysis and interpretation of data (e.g., statistical analysis, biostatistics, computational analysis): S. Whelan, E. Ophir, M.F. Kotturi, O. Levy, S. Ganguly, L. Leung, S. Kumar, L. Dassa, A. Soni, J.M. Taube, S.C. Liang
Writing, review, and/or revision of the manuscript: S. Whelan, E. Ophir, M.F. Kotturi, S. Ganguly, S. Kumar, L. Dassa, A. Soni, J.M. Taube, A.N. Fader, I.-M. Shih, D.M. Pardoll, S.C. Liang
Administrative, technical, or material support (i.e., reporting or organizing data, constructing databases): S. Whelan, L. Leung, B. Murter, T.-L. Wang
Study supervision: O. Levy, I. Vaknin, L. Dassa

Acknowledgments

This study was supported by NIH Research Grant T32CA193145 (to A. Soni); NCI CCSG grant P30 CA006973 (to S. Ganguly); NIH/NCI grants P50CA228991, RO1CA215483, and UO1CA200469, and the Ovarian Cancer Research Alliance (to L. Shih and T. Wang); NCI/NIH P50CA228991 and NCI/NIH RO1CA215483 (to T. Wang); and NCI R01 CA142779 (to J. M. Taube and D. M. Pardoll).

The costs of publication of this article were defrayed in part by the payment of page charges. This article must therefore be hereby marked *advertisement* in accordance with 18 U.S.C. Section 1734 solely to indicate this fact.

Received July 5, 2018; revised September 30, 2018; accepted December 5, 2018; published first January 18, 2019.

References

1. Hanahan D, Weinberg RA. The hallmarks of cancer. Cell 2000;100:57–70.
2. Hanahan D, Weinberg RA. Hallmarks of cancer: the next generation. Cell 2011;144:646–74.
3. Zarour HM. Reversing T-cell dysfunction and exhaustion in cancer. Clin Cancer Res 2016;22:1856–64.
4. Pardoll DM. The blockade of immune checkpoints in cancer immunotherapy. Nat Rev Cancer 2012;12:252–64.
5. Doering TA, Crawford A, Angelosanto JM, Paley MA, Ziegler CG, Wherry EJ. Network analysis reveals centrally connected genes and pathways involved in $CD8^+$ T cell exhaustion versus memory. Immunity 2012;37:1130–44.
6. Sharma P, Allison JP. Immune checkpoint targeting in cancer therapy: toward combination strategies with curative potential. Cell 2015;161:205–14.
7. Cha E, Klinger M, Hou Y, Cummings C, Ribas A, Faham M, et al. Improved survival with T cell clonotype stability after anti-CTLA-4 treatment in cancer patients. Sci Transl Med 2014;6:238ra70.
8. Robert L, Tsoi J, Wang X, Emerson R, Homet B, Chodon T, et al. CTLA4 blockade broadens the peripheral T-cell receptor repertoire. Clin Cancer Res 2014;20:2424–32.
9. Tumeh PC, Harview CL, Yearley JH, Shintaku IP, Taylor EJ, Robert L, et al. PD-1 blockade induces responses by inhibiting adaptive immune resistance. Nature 2014;515:568–71.
10. Zaretsky JM, Garcia-Diaz A, Shin DS, Escuin-Ordinas H, Hugo W, Hu-Lieskovan S, et al. Mutations associated with acquired resistance to PD-1 blockade in melanoma. N Engl J Med 2016;375:819–29.
11. Chan CJ, Andrews DM, Smyth MJ. Receptors that interact with nectin and nectin-like proteins in the immunosurveillance and immunotherapy of cancer. Curr Opin Immunol 2012;24:246–51.
12. Martinet L, Smyth MJ. Balancing natural killer cell activation through paired receptors. Nat Rev Immunol 2015;15:243–54.
13. Zhu Y, Paniccia A, Schulick AC, Chen W, Koenig MR, Byers JT, et al. Identification of CD112R as a novel checkpoint for human T cells. J Exp Med 2016;213:167–76.
14. Bottino C, Castriconi R, Pende D, Rivera P, Nanni M, Carnemolla B, et al. Identification of PVR (CD155) and Nectin-2 (CD112) as cell surface ligands for the human DNAM-1 (CD226) activating molecule. J Exp Med 2003;198:557–67.
15. Yu X, Harden K, Gonzalez LC, Francesco M, Chiang E, Irving B, et al. The surface protein TIGIT suppresses T cell activation by promoting the generation of mature immunoregulatory dendritic cells. Nat Immunol 2009;10:48–57.
16. Stanietsky N, Simic H, Arapovic J, Toporik A, Levy O, Novik A, et al. The interaction of TIGIT with PVR and PVRL2 inhibits human NK cell cytotoxicity. Proc Natl Acad Sci USA 2009;106:17858–63.

17. Johnston RJ, Comps-Agrar L, Hackney J, Yu X, Huseni M, Yang Y, et al. The immunoreceptor TIGIT regulates antitumor and antiviral CD8(+) T cell effector function. Cancer Cell 2014;26:923–37.
18. Zhang B, Zhao W, Li H, Chen Y, Tian H, Li L, et al. Immunoreceptor TIGIT inhibits the cytotoxicity of human cytokine-induced killer cells by interacting with CD155. Cancer Immunol Immunother 2016;65:305–14.
19. Johnston RJ, Yu X, Grogan JL. The checkpoint inhibitor TIGIT limits antitumor and antiviral CD8(+) T cell responses. Oncoimmunology 2015;4:e1036214.
20. Chan CJ, Martinet L, Gilfillan S, Souza-Fonseca-Guimaraes F, Chow MT, Town L, et al. The receptors CD96 and CD226 oppose each other in the regulation of natural killer cell functions. Nat Immunol 2014;15:431–8.
21. Fuchs A, Cella M, Giurisato E, Shaw AS, Colonna M. Cutting edge: CD96 (tactile) promotes NK cell-target cell adhesion by interacting with the poliovirus receptor (CD155). J Immunol 2004;172:3994–8.
22. Xu F, Sunderland A, Zhou Y, Schulick RD, Edil BH, Zhu Y. Blockade of CD112R and TIGIT signaling sensitizes human natural killer cell functions. Cancer Immunol Immunother 2017.
23. Leitner J, Kuschei W, Grabmeier-Pfistershammer K, Woitek R, Kriehuber E, Majdic O, et al. T cell stimulator cells, an efficient and versatile cellular system to assess the role of costimulatory ligands in the activation of human T cells. J Immunol Methods 2010;362:131–41.
24. Deuss FA, Gully BS, Rossjohn J, Berry R. Recognition of nectin-2 by the natural killer cell receptor T cell immunoglobulin and ITIM domain (TIGIT). J Biol Chem 2017;292:11413–22.
25. Linsley PS, Bradshaw J, Greene J, Peach R, Bennett KL, Mittler RS. Intracellular trafficking of CTLA-4 and focal localization towards sites of TCR engagement. Immunity 1996;4:535–43.
26. Alegre ML, Noel PJ, Eisfelder BJ, Chuang E, Clark MR, Reiner SL, et al. Regulation of surface and intracellular expression of CTLA4 on mouse T cells. J Immunol 1996;157:4762–70.
27. Tsao MS, Kerr KM, Kockx M, Beasley MB, Borczuk AC, Botling J, et al. PD-L1 immunohistochemistry comparability study in real-life clinical samples: results of blueprint phase 2 project. J Thorac Oncol 2018;13:1302–11.
28. Li Y, Liang L, Dai W, Cai G, Xu Y, Li X, et al. Prognostic impact of programed cell death-1 (PD-1) and PD-ligand 1 (PD-L1) expression in cancer cells and tumor infiltrating lymphocytes in colorectal cancer. Mol Cancer 2016;15:55.
29. Sabatier R, Finetti P, Mamessier E, Adelaide J, Chaffanet M, Ali HR, et al. Prognostic and predictive value of PDL1 expression in breast cancer. Oncotarget 2015;6:5449–64.
30. Valk E, Rudd CE, Schneider H. CTLA-4 trafficking and surface expression. Trends Immunol 2008;29:272–9.
31. Murter B. Mouse PVRIG has $CD8^+$ T cell–specific coinhibitory functions and dampens antitumor immunity. Cancer Immunol Res 2019;7:244–56.
32. Ahmadzadeh M, Johnson LA, Heemskerk B, Wunderlich JR, Dudley ME, White DE, et al. Tumor antigen-specific CD8 T cells infiltrating the tumor express high levels of PD-1 and are functionally impaired. Blood 2009;114:1537–44.
33. Kovacsovics-Bankowski M, Chisholm L, Vercellini J, Tucker CG, Montler R, Haley D, et al. Detailed characterization of tumor infiltrating lymphocytes in two distinct human solid malignancies show phenotypic similarities. J Immunother Cancer 2014;2:38.
34. Daud AI, Wolchok JD, Robert C, Hwu WJ, Weber JS, Ribas A, et al. Programmed death-ligand 1 expression and response to the anti-programmed death 1 antibody pembrolizumab in melanoma. J Clin Oncol 2016;34:4102–9.
35. Oshima T, Sato S, Kato J, Ito Y, Watanabe T, Tsuji I, et al. Nectin-2 is a potential target for antibody therapy of breast and ovarian cancers. Mol Cancer 2013;12:60.
36. Cerboni C, Fionda C, Soriani A, Zingoni A, Doria M, Cippitelli M, et al. The DNA damage response: a common pathway in the regulation of NKG2D and DNAM-1 ligand expression in normal, infected, and cancer cells. Front Immunol 2014;4:508.
37. de Andrade LF, Smyth MJ, Martinet L. DNAM-1 control of natural killer cells functions through nectin and nectin-like proteins. Immunol Cell Biol 2014;92:237–44.
38. Taube JM, Anders RA, Young GD, Xu H, Sharma R, McMiller TL, et al. Colocalization of inflammatory response with B7-h1 expression in human melanocytic lesions supports an adaptive resistance mechanism of immune escape. Sci Transl Med 2012;4:127ra37.
39. Schalper KA, Carvajal-Hausdorf D, McLaughlin J, Altan M, Velcheti V, Gaule P, et al. Differential expression and significance of PD-L1, IDO-1, and B7-H4 in human lung cancer. Clin Cancer Res 2017;23:370–8.